Nonlinear Amplification of Stationary Rossby Waves near Resonance. Part II

P. MALGUZZI

CNR–FISBAT, Bologna, Italy

A. SPERANZA

Universita' di Camerino, Camerino, Italy

A. SUTERA AND R. CABALLERO

Universita' La Sapienza, Rome, Italy

(Manuscript received 7 February 1996, in final form 16 January 1997)

ABSTRACT

In a preceding paper the authors showed that planetary waves of very different amplitudes can be sustained on the same configuration of the zonal wind by asymptotically balancing the energy contributions related to Ekman dissipation and orographic drag. The basic physical mechanism considered, namely, nonlinear self-interaction of the eddy field, was modeled in a vertically continuous quasigeostrophic model by means of a perturbative approach that relies on an ad hoc choice of the meridional profile of the wave field itself. Given the mathematical limitations of this approach, some important aspects of the mechanism of resonance bending were not explored; in particular, the sensitivity of stationary solutions to changes in the zonal wind profile, channel geometry, and physical parameters such as dissipation coefficients and mountain height.

In the present paper, the robustness of the mechanism of resonance folding by numerical means is analyzed, in the framework of both the barotropic and the two-level quasigeostrophic model. It is demonstrated that resonance bending is a generic property of the equations governing atmospheric motions on the planetary scale. In particular, it is shown that multiple stationary solutions can be achieved with realistic values of Ekman dissipation and mountain height in the context of the two-level quasigeostrophic model.

The authors formulate a weakly nonlinear theory that does not rely on any a priori assumptions about the meridional structure of the solution. Numerical and analytical results are compared, obtaining a satisfactory agreement in the parameter range in which the asymptotic theory is valid. The authors conclude that the present model is still a good candidate for the explanation of one of the most relevant statistical property of low-frequency variability at midlatitudes, namely, that large amplitude fluctuations of ultralong waves correspond to small variations of the zonal wind.

1. Introduction

Research on the nature of flow regimes is potentially important in understanding persistence and predictability of atmospheric motion beyond the timescales typical of baroclinic synoptic disturbances. In fact, slower evolving planetary patterns are crucial in determining seasonal anomalies and, therefore, weather evolution on these timescales. The potential benefits in understanding the dynamics of these timescales has led many investigators to study the organization of the global atmospheric motion, renewing the interest in the weather regimes concept. Regardless of the method employed in the classification of weather regimes, a common feature shown in many studies is that transitions among regimes occur on timescales (3–4 days) shorter than the average persistence time of any of them. Moreover, limiting the attention to the planetary-scale component of the flow, a shift from one regime to another implies changes of several decameters in the geopotential height, often achieved by a virtually unpropagating amplification of the planetary-scale eddy field.

The above phenomenology suggests that the relevant physical mechanism responsible for weather regimes should be characterized by a zero phase velocity wave growth and persistence. A natural candidate for this process is the interaction between eddy field and topography on the planetary scale, which, as known since Charney and Eliassen (1949), is characterized by a nonpropagating amplification of the eddy field. However, it still is an open question whether topography is able to determine atmospheric fluctuations in distinct, persistent, and nonpropagating planetary-scale weather regimes. Along these lines, Hansen and Sutera (1995)

Corresponding author address: Dr. Piero Malguzzi, CNR–FISBAT, via Gobetti 101, 40129 Bologna, Italy.

have shown that the modification of the topographic height leads, in a GCM long run, to the generation of two distinct weather regimes, consistent with what was suggested by the studies of Charney and Devore (1979), Wiin-Nielsen (1979), and many others. In particular, Benzi et al. (1986) suggested that, in a simple model of an orographically induced eddy field, multiple weather regimes might be created if the nonlinear nature of wave interaction is accounted for.

In Malguzzi et al. (1996, hereafter referred to as Part I), it was shown that large, multiple-amplitude planetary waves can be maintained by balancing asymptotically small Ekman dissipation and orographic drag. This effect was illustrated in a vertically continuous quasigeostrophic model by means of perturbative calculations along the line proposed by Benzi et al. (1986, hereafter referred to as BMSS). However, in BMSS the effect of wave self-interaction, responsible for the multiplicity of solutions, was parameterized by an ad hoc choice of the meridional structure of the eddy streamfunction field. In Part I, by numerically solving for the stationary solutions of a barotropic model near orographic resonance, it was shown that BMSS's assumption was justified, when spherical geometry is considered, even in the case of eddies superimposed on a uniform zonal wind.

In Part I, three main aspects of the problem were left open. The first one was related to the sensitivity of the solution to physical parameters (in particular, the zonal wind profile and the channel width) and numerical resolution employed in the finite difference scheme used to solve the governing equations. In the present paper this question is addressed by means of further numerical calculations.

The second point had to do with the unrealistic choice of some parameters (Ekman dissipation timescale and orographic height were exceedingly small) used to obtain bended resonance and multiple solutions in the barotropic framework. As suggested by the analytical argument developed for the vertically continuous model, in a baroclinic framework, owing to the fact that low-level eddy wave amplitude and zonal wind are much smaller than the corresponding midtropospheric quantities, small dissipation and orographic drag can be obtained for more realistic values of the above parameters. Unfortunately, the vertically and meridionally continuous model could not be solved numerically because its phase space dimension would be too large to be handled. Hence, in the present paper, a two-layer quasigeostrophic model is studied with a particular physical parameter setting that allows us to compare results with the vertically continuous model presented in part I.

Finally, the analytical theory of BMSS is reformulated without the limiting assumption of a priori specified meridional structure. The comparison between the predictions of the new theory and the numerical solutions, obtained for the barotropic case, proves very satisfactory. In particular, the revised theory accounts for some features of the resonance curve (like bending to the left) that could not be predicted by strict use of BMSS calculations.

The present paper is organized as follows. In section 2, the robustness of the numerical solutions of the barotropic model studied in Part I is assessed. In particular, multiple numerical solutions are obtained for the case in which the zonal wind is specified from an observed midtropospheric winter profile, extending from 20°N to the North Pole. In section 3, by means of a simple two-layer model, it is shown that resonance bending can be obtained with realistic values of Ekman dissipation and orographic height. Numerical solutions are given for different wind profiles, channel width, and horizontal resolution. In section 4, the revised, weakly asymptotic theory of BMSS is presented. In section 5, the predictions of the theory are checked against the numerical solution obtained in the barotropic and baroclinic cases. Finally, in section 6, the conclusions are drawn.

2. Barotropic model

In Part I (section 3) we computed the resonance structure for the numerical solution of a barotropic model [Eq. (4) in Part I] in a spherical channel. The solutions are obtained by defining the zonal wind $U(\phi)$ according to the formula

$$U(\phi) = uP(\phi), \tag{1}$$

while solution curves are computed by varying the parameter u through linear resonance. In the previous equation, $P(\phi)$ is a latitudinal profile normalized to a maximum amplitude of 1. In Part I we considered two simple profiles in a 30° wide channel centered at 45°N, namely, $P = 1$ and a sine function with zero values at 25° and 65°N. The orographic elevation was defined by the simple analytical form

$$h(\phi, \lambda) = h_o \sin\left(\frac{\phi - 30^\circ}{30^\circ}\pi\right) e^{in_R\lambda} + \text{c.c.}, \tag{2}$$

where c.c. stands for complex conjugate and $n_R = 3$. Expression (2) defines a sinusoidal orography vanishing at the latitudinal walls of the spherical channel and with maximum amplitude of $2h_o$. The total streamfunction of the problem was decomposed into a zonal and eddy part,

$$\Psi = -\int_{\phi_o}^{\phi} Ua\, d\phi + \sum_{n=1}^{\text{NT}} \Psi_n(\phi) e^{in\lambda} + \text{c.c.}, \tag{3}$$

where the Fourier coefficients of the eddy streamfunction field were further discretized on a meridional grid of J points equally spaced. The resulting $2 \times \text{NT} \times J$ nonlinear algebraic equations were solved numerically with a Newton–Keller pseudo-arclength continuation method; meridional and zonal resolution were set to $J = 20$ and $\text{NT} = 2n_R = 6$.

In the present section, we present a study on the sensitivity of the numerical solutions obtained in Part I with

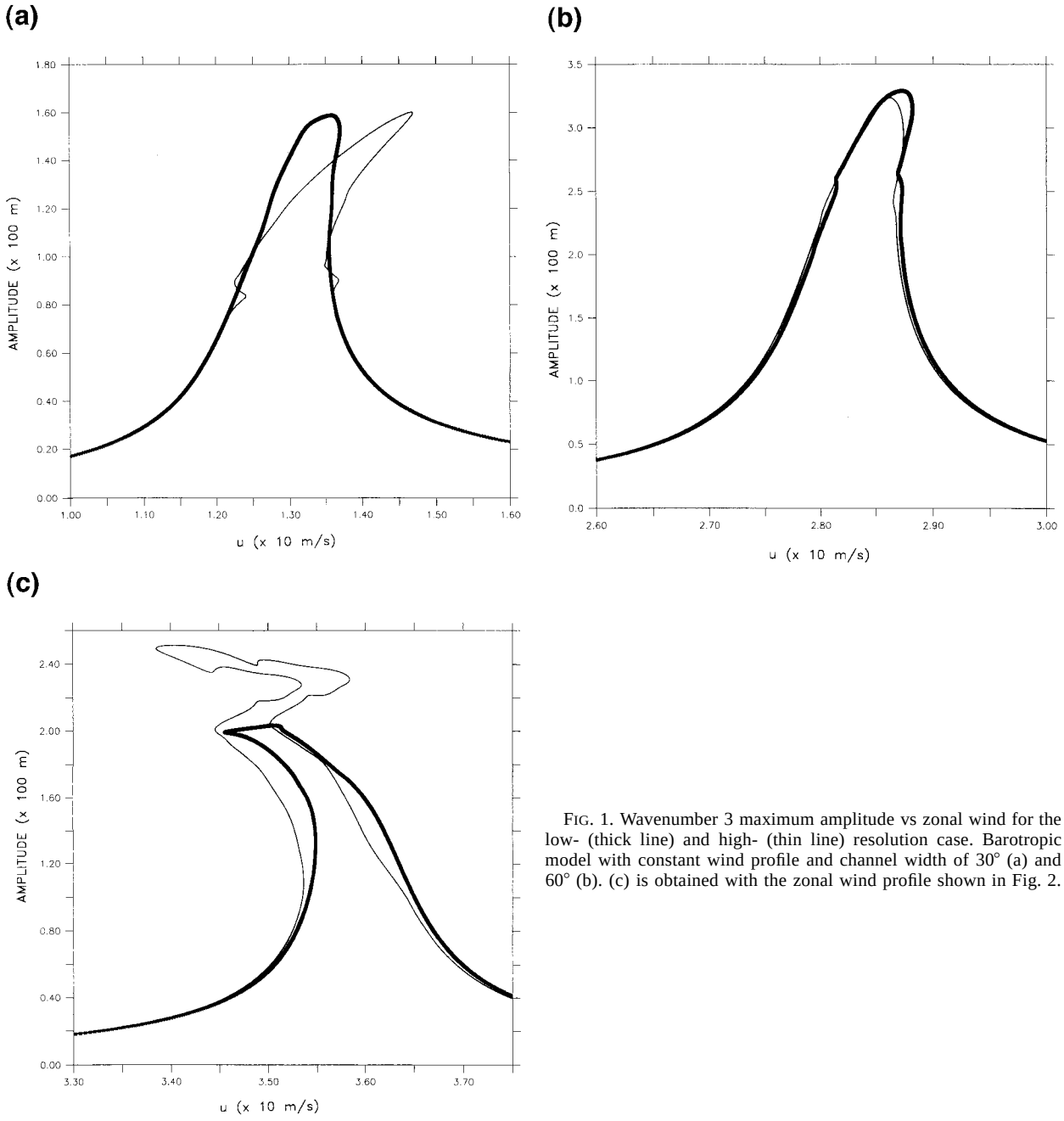

FIG. 1. Wavenumber 3 maximum amplitude vs zonal wind for the low- (thick line) and high- (thin line) resolution case. Barotropic model with constant wind profile and channel width of 30° (a) and 60° (b). (c) is obtained with the zonal wind profile shown in Fig. 2.

respect to variations of channel width and meridional and zonal resolution. Resonance curves are also obtained in the case of zonal wind profiles specified from observations. Figures 1a, b, c show the resonance curve (maximum of $|\Psi n_R|$ vs u) for the cases $P = 1$, channel width 30° (Fig. 1a); $P = 1$, channel width 60° (Fig. 1b); and $P(\phi)$ obtained from the zonally averaged zonal wind averaged over the month of January 1967 (Fig. 1c). In the latter case, the meridional domain extends from 20°N to the North Pole (see Fig. 2), while the zonal wind is computed from the observed 500-mb geopotential height [National Meteorological Center (NMC, now known as the National Centers for Environmental Prediction) data] using the geostrophic relationship. Each figure shows two curves that correspond to resolution NT = 6, $J = 20$ (thick solid line) and NT = 18, $J = 60$ (thin line). Of course, owing to the simple longitudinal dependence of the topography, only integer multiples of n_R are present in the solution. In all cases, the Ekman dissipation coefficient is set to $\nu_E = 0.01$ (roughly 100 days of e-folding time: dimensionless quantities are scaled as in Part I) and a superdissipative

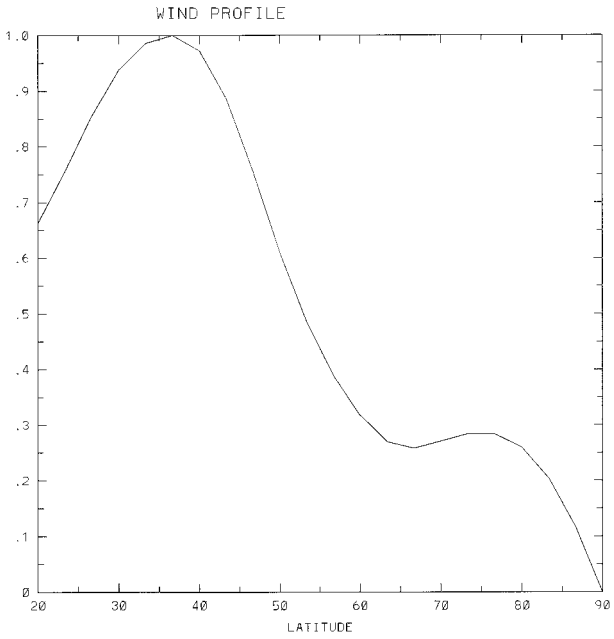

FIG. 2. Normalized zonal wind profile obtained from the average over the month of January 1967.

term of the form $\nu_{sd}\nabla^4\Psi$, with $\nu_{sd} = 0.002$, is inserted in the right-hand side of the barotropic equation [see Eq. (4) of Part I] to prevent the occurrence of noisy numerical solutions and to ensure convergence with increasing resolution. The topographic elevation is set to $h_o = 0.06$ (corresponding to a maximum dimensional height of 120 m) in Fig. 1a, $h_o = 0.02$ in Fig. 1b, and $h_o = 0.01$ in Fig. 1c. In the latter two cases we have specified unrealistically low values for the mountain height; the reason is that in Figs. 1b and 1c resonance is located at unrealistically large values of the zonal wind, so that mountain drag becomes significant even for small orography. As we will see in the next section, this will not be the case in the baroclinic framework.

On the basis of the results depicted in Fig. 1 we conclude that resonance folding is a generic property of this model. The low-resolution curve of Fig. 1a is essentially the same as Fig. 3a of Part I, although here the orographic height is slightly larger. In some cases, the increase of resolution introduces complicated features in the resonance curve, like multiple foldings and, probably, branches separation. Unfortunately, the occurrence of isolated solution branches, requiring the specification of accurate first guesses in a large dimension phase space, is very difficult to handle with the present technique. For instance, the high-resolution curve of Fig. 1a shows two bumps at amplitude of about 0.8, which become more pronounced by reducing the mountain height (not shown), eventually cutting out the upper part of the resonance. A similar behavior is observed in Fig. 1c, where the low-resolution curve is sharply cut at amplitude values just above 2.0. The search for an isolated solution branch (suspected) at amplitude of about 2.5 was, however, unsuccessful in this case. The case of Fig. 1b (large channel width) shows little modification with increasing resolution.

3. The baroclinic model

In this section we address two questions. First, we want to assess the sensitivity of resonance folding to parameter variations in the two-layer quasigeostrophic model, similar to what was done in the previous section for the barotropic model. Then we show that, in a baroclinic framework, we can specify more realistic values of Ekman dissipation, topographic height, and zonal wind strength and still obtain multiple stationary solutions and folded resonance curves. This possibility was anticipated in Part I in the context of a vertically continuous model solved by analytical methods; here we address the problem by numerical means, using the same Newton–Keller technique already applied in the barotropic case. The model is

$$J(\Psi_1, \nabla^2\Psi_1 + F_1(\Psi_2 - \Psi_1) + f) = -\frac{\nu_s}{2}\nabla^2(\Psi_1 - \Psi_2) + F_1\nu_H(\Psi_1 - \Psi_2) + \nu_{sd}\nabla^4\Psi_1$$

$$J(\Psi_2, \nabla^2\Psi_2 + F_2(\Psi_1 - \Psi_2) + f + h) = \frac{\nu_s}{2}\nabla^2(\Psi_1 - \Psi_2) - F_2\nu_H(\Psi_1 - \Psi_2) - \nu_E\nabla^2\Psi_2 + \nu_{sd}\nabla^4\Psi_2 \quad (4)$$

$$F_{1,2} = \frac{f_o^2 L^2}{g\frac{\Delta\rho}{\rho_o}D_{1,2}}, \qquad \nu_E = \frac{(A_\nu f_o)^{1/2}}{2U}\frac{L}{D_2},$$

where Ψ_1 (Ψ_2) denotes the upper (lower) layer total streamfunctions; D_1 (D_2), the upper (lower) layer thickness; F_1 (F_2), the upper (lower) layer Froude number; ν_H, the Newtonian cooling coefficient; ν_s, the internal momentum drag coefficient; and where the other symbols have the meaning introduced previously.

Here we use two different Froude numbers. Their values are chosen in such a way that the interaction between wind and topography is confined in a shallow layer, as it would be the case in the vertically continuous model. In fact, a small ratio, F_1/F_2, implies a shallow lower layer, F_1/F_2, being equal to D_2/D_1 (Pedlosky 1987). It is useful to mention that Eq. (4) is written in dimensionless form and that the orography is scaled with the product of the Rossby number times the lower-layer thickness. To fix ideas, $h = 1.0$ corresponds to a real topography of 200-m height if $F_1/F_2 = ¼$ and the height scale is 10 km. The four dissipation parameters are fixed at $\nu_E = 0.1$ (e-folding time of about 10 days), $\nu_S = \nu_H = 0.02$ (50 days), and $\nu_{sd} = 0.002$.

Similarly to the barotropic case, the upper- and lower-layer streamfunctions are decomposed in Fourier series along latitude circles as

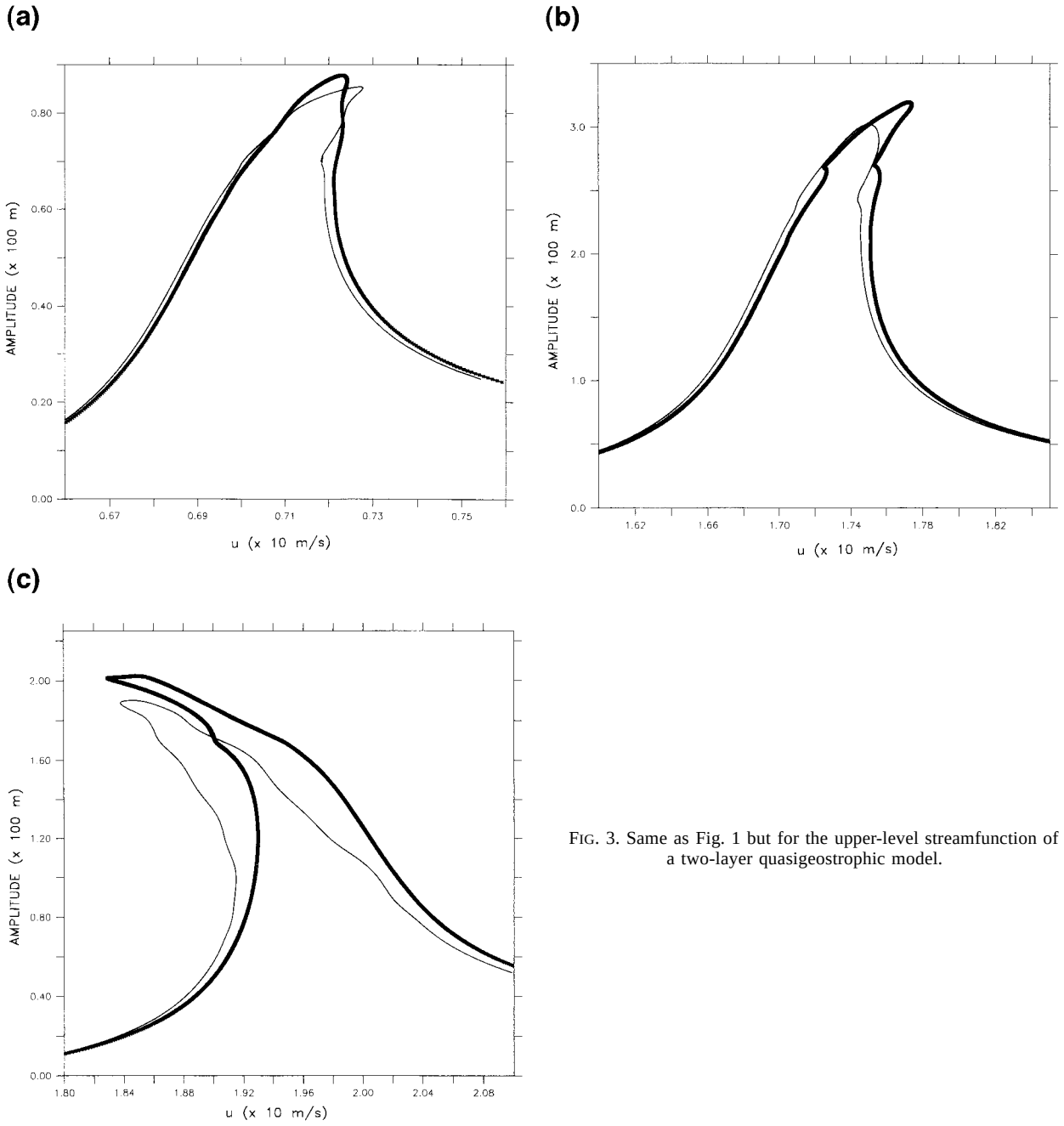

FIG. 3. Same as Fig. 1 but for the upper-level streamfunction of a two-layer quasigeostrophic model.

$$\Psi_{1,2} = -\int_{\phi_o}^{\phi} aU_{1,2}\, d\phi + \sum_{n=1}^{\mathrm{NT}} \Psi_n^{(1,2)} e^{in\lambda} + \text{c.c.}, \quad (5)$$

where U_1 (U_2) denotes the upper (lower) zonal wind profile. The meridional profiles of each zonal wavenumber is then discretized, and the resulting set of nonlinear algebraic equations are solved numerically as before. Solution curves are obtained by fixing the same profile of the zonal wind in the upper and lower layer as

$$U_{1,2} = u_{1,2}P(\phi), \quad (6)$$

and by varying the parameter $u = (u_1 + u_2)/2$ for a specified vertical shear, $u_s = (u_1 - u_2)/2$. The orography is still specified according to Eq. (2) of the previous section.

Figures 3a,b,c show the stationary solutions for the same channel width, wind profile, and numerical resolution used in the barotropic case illustrated in the previous section. The remaining parameters are set to: $h_o = 0.4$, $F_1 = 1.0$, $F_2 = 5.0$, $u_s = 0.6$ in Fig. 3a; h_o

$= 0.4$, $F_1 = 1.0$, $F_2 = 5.0$, $u_s = 1.2$ in Fig. 3b; and $h_o = 0.3$, $F_1 = 1.0$, $F_2 = 4.0$, $u_s = 1.7$ in Fig. 3c.

The results are very similar to the ones previously discussed, not surprisingly due to the large ratio between F_1 and F_2. Again, the case with the real wind profile exhibits a subresonant folding, but now resonance occurs at realistic values of the zonal wind (the actual value of u that matches the 500-hPa zonal wind from which P is defined is around 2.0 dimensionless units).

The two-layer model is an accurate description of a very simple, realizable physical system. However, system (4) can also be viewed as a finite-difference approximation of a vertically continuous physical system [two-level model; see Pedlosky (1987)]. Therefore, it is interesting to see how the stationary solutions of (4) behave in the more classic case in which $F_1 = F_2 = F = f_o^2 L^2/(N^2 D^2)$, where N is the Brunt–Väisälä frequency, and where $D = D_1 = D_2$. By assuming a standard stratification of 50° in 10 km and $D = 5$ km, it turns out $F = 2.4$. The Ekman coefficient is set to the more realistic value of 0.23, corresponding to 5 days of e-folding time. The meridional profile P of the zonal wind is specified as a sine function centered at 45° and zeros at 20° and 70°. The meridional extension of the domain is set to 40°, with lateral walls located at 25° and 65°; as discussed in Part I, this is done in order to avoid critical levels at the side boundaries. Orography is specified according to expression (2), but in the wider channel, while the other parameters are set to $u_S = 1.7$ (17 m s^{-1}), $\nu_S = \nu_H = 0.11$ (10 days), and $\nu_{sd} = 0.002$. Horizontal resolution is set to NT = 6 and $J = 40$. Figures 4a,b show the maximum streamfunction amplitude and the phase of zonal wavenumber 3 in the upper level versus the zonal wind u, obtained with $h_o = 0.05$ (maximum mountain height of 50 m) and $h_o = 0.15$ (150 m). The interesting feature is that, for small values of orographic elevation, an ''island'' of large amplitude stationary solutions detachs from the main resonant branch. The isolated branch, which collapses to a single point in the limit of vanishing orography, appears for reasonable values of the zonal wind, namely, 3–4 m s^{-1} maximum speed in the lower level and 37 m s^{-1} in the upper one. We will return to this case in section 5 where we compare numerical and analytical results.

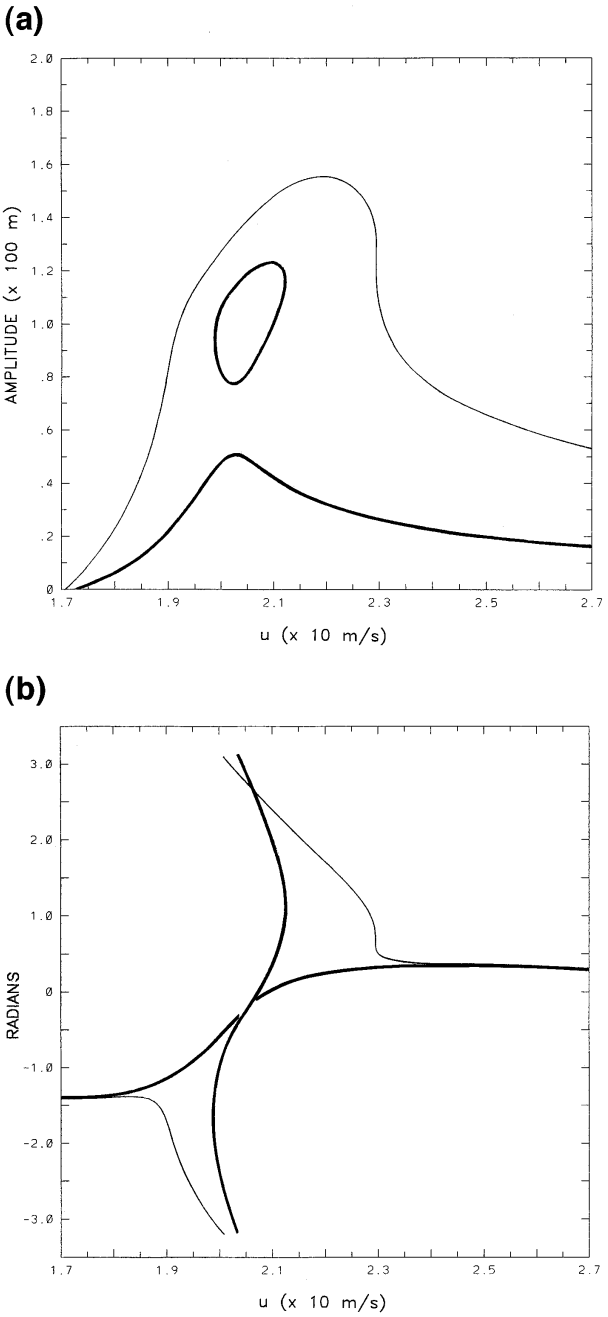

FIG. 4. Maximum amplitude (a) and phase (b) of zonal wavenumber 3 in the upper level vs the zonal wind u. Thick (thin) solid line is for $h_0 = 0.05$ ($h_0 = 0.15$).

4. Weakly nonlinear theory of resonance

In this section, we reformulate BMSS's theory with no a priori specification of the meridional structure of the solution; however, we still assume meridional confinement by lateral walls. For simplicity, we consider the barotropic vorticity equation in spherical coordinates (the generalization to the two-level model is straightforward):

$$\partial_t \nabla^2 \Psi + J(\Psi, \nabla^2 \Psi + f + h) = -\nu_E \nabla^2 \Psi, \quad (7)$$

where the symbols have the usual meaning. We look for stationary solutions of Eq. (7). The total streamfunction is decomposed into zonal mean and eddy part as

$$\Psi = -\int_{\phi_o}^{\phi} Ua \, d\phi + \Psi'(\lambda, \phi), \quad (8)$$

where, by definition, Ψ' has zero longitudinal mean. The shape of stationary eddies is then given by

$$U\partial_\lambda \nabla^2\Psi' + \partial_\lambda\Psi'[\beta - U_{yy}] + a\cos\phi J(\Psi', \nabla^2\Psi' + h) + U\partial_\lambda h = -\nu_E a\cos\phi\nabla^2\Psi', \quad (9)$$

where

$$\beta = \frac{2\Omega\cos\phi}{a}, \qquad U_{yy} = \partial_\phi\left[\frac{1}{a^2\cos\phi}\partial_\phi(\cos\phi U)\right], \quad (10)$$

and where we assume that $U(\phi)$ is fixed (we do not consider the equation for the zonal wind).

We are going to solve Eq. (9) in the asymptotic limit of small orographic forcing and in the near resonant case. Let h (orography) denote the small parameter. Close to resonance, the amplitude is limited only by dissipation. Hence, $\nu_E\Psi'$ should be of order h as well, so that the order of magnitude of the solution depends on the hypothesis we made of the magnitude of ν_E. For instance, ν_E of order 1 implies a solution of order h (no large-amplitude response can be obtained in this case), while ν_E of order h implies a solution of order 1. Unfortunately, in the latter case we do not expect to be able to solve analytically Eqs. (9) and (10) because nonlinearity is not perturbative. Hence, we study the case in which the order of magnitude of ν_E is between h and 1; as always in perturbative expansions, we hope that the solution obtained in this particular parameter range gives useful indications also for the more general case.

For the sake of clarity, we anticipate that the consistent scaling is ν_E of order $h^{2/3}$ and Ψ' of order $h^{1/3}$. It remains to be seen how close to resonance (i.e., the order of magnitude of the difference, say, $\Delta\mu$, between the orographic and the internal stationary wavenumber) we have to go to obtain solutions of order $h^{1/3}$. This aspect of the problem will be defined as the asymptotic expansion proceeds. Hence, let $\Psi' = \Psi'^{(0)} + \Psi'^{(1)} + \Psi'^{(2)} + \cdots$, where $\Psi'^{(l)}$ is of order $h^{(l+1)/3}$.

Since $h^{1/3}$ is still much smaller than unity, the eddy streamfunction is governed, at the lowest order, by the well-known linear problem of Rossby wave propagation

$$U\partial_\lambda\nabla^2\Psi'^{(0)} + \partial_\lambda\Psi'^{(0)}(\beta - U_{yy}) = 0. \quad (11)$$

The solution of (11) can be written in the form

$$\Psi'^{(0)} = A(\Lambda)g(\phi)e^{i\mu\lambda} + \text{c.c.} \qquad \Lambda = \Delta\mu\lambda, \quad (12)$$

where u denotes the internal stationary wavenumber, A the order $h^{1/3}$ (so far arbitrary) amplitude that is a function of the slow longitudinal coordinate Λ, and where the $O(1)$ function g denotes the meridional structure. The slow-amplitude modulation is needed to match the longitudinal variation of orography, which, in near resonant conditions, is asymptotically close to $e^{i\mu\lambda}$. Therefore, the eddy streamfunction will be basically a linear and stationary Rossby wave with a zonal wavenumber equal to that of the orography.

By substituting (12) into (11) we get the problem determining the meridional structure $g(\phi)$:

$$\frac{1}{a^2\cos\phi}\partial_\phi[\cos\phi\partial_\phi g] - V(\phi)g - \frac{\mu^2}{a^2\cos^2\phi}g = 0.$$

$$V(\phi) = -\frac{\beta - U_{yy}}{U}. \quad (13)$$

Problem (13) becomes an eigenvalue problem (the eigenvalue being the square of the internal zonal wavenumber) if homogeneous boundary conditions are assumed in the meridional direction. Therefore, we shall assume that g vanishes at certain latitudes, say, ϕ_0 and ϕ_1, implying confinement in the meridional direction. Finally, we are free to choose a normalization of g by setting

$$\int_{\phi_0}^{\phi_1} d\phi\,\frac{g^2}{\cos\phi} = 1. \quad (14)$$

The next term entering the asymptotic expansion at order $h^{2/3}$ is the Jacobian of the Rossby wave. Hence, the first-order correction to (12) is given by

$$U\partial_\lambda\nabla^2\Psi'^{(1)} + \partial_\lambda\Psi'^{(1)}[\beta - U_{yy}] = -a\cos\phi J(\Psi'^{(0)}, \nabla^2\Psi'^{(0)}). \quad (15)$$

The solution of (15) can be written as

$$\Psi'^{(1)} = A^2 p(\phi)e^{2i\mu\lambda} + \text{c.c.}, \quad (16)$$

where the real function $p(\phi)$ satisfies

$$\frac{1}{a^2\cos\phi}\partial_\phi(\cos\phi\partial_\phi p) - Vp - \frac{4\mu^2}{a^2\cos^2\phi}p = -\frac{g^2\partial_\phi V}{2aU}, \quad (17)$$

and where the zero order equation (13) has been used in the evaluation of the right-hand side of (15). The above linear equation can be solved once a particular eigenvalue and eigenvector of (13) are chosen; its solution gives the meridional structure $p(\phi)$ of the zonal wavenumber 2μ, which is directly forced by the Jacobian of the zero-order solution.

The second-order correction $\Psi'^{(2)}$ is governed, at order h, by

$$U\partial_\lambda\nabla^2\Psi'^{(2)} + \partial_\lambda\Psi'^{(2)}[\beta - U_{yy}] = -\frac{2U\Delta\mu}{a^2\cos^2\phi}\partial_{\lambda\lambda\Lambda}\Psi'^{(0)} - a\cos\phi J(\Psi'^{(1)}, \nabla^2\Psi'^{(0)}) - a\cos\phi J(\Psi'^{(0)}, \nabla^2\Psi'^{(1)}) - U\partial_\lambda h - \nu_E a\cos\phi\nabla^2\Psi'^{(0)}, \quad (18)$$

where we have used the chain rule of derivation, namely,

$$\partial_\lambda\Psi'^{(0)} \to \partial_\lambda\Psi'^{(0)} + \partial_\Lambda\Psi'^{(0)}\frac{d\Lambda}{d\lambda},$$

$$\partial_{\lambda\lambda}\Psi'^{(0)} \to \partial_{\lambda\lambda}\Psi'^{(0)} + 2\partial_{\lambda\lambda}\Psi'^{(0)}\frac{d\Lambda}{d\lambda} + O(\Delta\mu^2). \quad (19)$$

Note that the Jacobian of the zero-order solution with

topography should be neglected because it is of higher order ($h^{4/3}$). Equation (18) also determines the condition of near resonance; only when the detuning from resonance, $\Delta\mu$, is order $h^{2/3}$ does the first term on the right-hand side of (18) become as important as the other ones.

We must now specify the form of the orography. Since we are in near-resonant conditions, we shall consider only the Fourier component with zonal wavenumber close to μ. Hence, following Eq. (2),

$$h(\lambda, \phi) = h_M(\phi)e^{in_R\lambda} + \text{c.c.} = h_M e^{i\Lambda}e^{i\mu\lambda} + \text{c.c.}$$
$$\Lambda = \Delta\mu\lambda, \qquad n_R - \mu \equiv \Delta\mu \leq O(h^{2/3}), \tag{20}$$

where $h_M(\phi)$ is the meridional profile of zonal wavenumber n_R (in general, a complex function).

The second-order correction is the superposition of zonal wavenumbers μ and 3μ. Since $e^{i\mu\lambda}$ is already a solution of the left-hand side of (18), a (necessary and sufficient) solvability condition will have to be satisfied for the solution of (18) to exist. This condition is obtained by imposing that the projection of the right-hand side of (18) on the solution of the adjoint of the zero-order problem (viz., $g\cos\phi e^{-i\mu\lambda}$) vanish. The derivation of this condition (sketched below for the interested reader) involves only straightforward algebra and leads to the final conditions (23) and (24).

Since only those terms proportional to $e^{i\mu\lambda}$ will give rise to nonvanishing scalar products, we only take into account the wavenumber μ Fourier component of (18). By letting

$$\Psi'^{(2)} = s(\phi)e^{i\mu\lambda} + \text{c.c.} + \cdots, \tag{21}$$

and by substituting (20) and (21) into (18), we get

$$\frac{1}{a^2\cos\phi}\partial_\phi(\cos\phi\partial_\phi s) - \frac{\mu^2 s}{a^2\cos^2\phi} - Vs$$
$$= -\frac{2i\mu\Delta\mu\partial_\Lambda A}{a^2\cos^2\phi}g - \frac{|A|^2A}{Ua}$$
$$\times\left\{\frac{g}{2a}\partial_\phi\left(\frac{g^2}{U}\partial_\phi V\right) + pg\partial_\phi V + \frac{1}{Ua}g^2\partial_\phi g\partial_\phi V\right\}$$
$$- h_M e^{i\Lambda} - \frac{\nu_E}{i\mu U}a\cos\phi AVg. \tag{22}$$

The necessary and sufficient condition for the solvability of (22) is obtained by projecting over $g\cos\phi$. By setting $A = A_o e^{i\Lambda}$, we finally get the algebraic relation for the amplitude equilibration:

$$A = A_o e^{i\Lambda}, \qquad I_\delta A_o|A_o|^2 - iA_o I_\nu - \frac{2\mu\Delta\mu}{a^2}A_o + I_h = 0, \tag{23}$$

where

$$I_h = \int_{\phi_0}^{\phi_1} gh_M\cos\phi\, d\phi,$$
$$I_\nu = \int_{\phi_0}^{\phi_1} \frac{\nu_E}{U\mu}a\cos^2\phi Vg^2\, d\phi,$$
$$I_\delta = \int_{\phi_0}^{\phi_1} \frac{\cos\phi}{Ua}\left[pg^2\partial_\phi V + \partial_\phi\left(\frac{g^4}{2Ua}\partial_\phi V\right)\right] d\phi. \tag{24}$$

By solving (23), the computation of the zero- and first-order solution is now complete. Equations (23) and (24) are the generalization of BMSS's theory to the case in which the zonal wind is a function of the meridional coordinate. Moreover, (23) and (24) have been derived without assuming any kind of meridional truncation, which was the main hindrance of the previous theory. The linear and topographic terms are identical to those of BMSS, while the expression of the coefficient of the cubic term is a complex function of the zonal wind meridional shear. In particular, the sign of I_δ can be positive or negative, implying sub- or superresonant foldings, while BMSS only predicted superresonant foldings.

In the following section, we compare the theory predictions with the numerical solutions obtained in sections 2 and 3.

5. Theory validation

We now assess the performance of the weakly nonlinear theory by checking its predictions against the numerical solutions presented in section 2. We solve numerically the eigenvalue problem (13), obtaining the meridional structure g, normalized according to (14), and the resonant wavenumber μ. Then, we solve the linear problem (17) for the meridional structure p of the zonal wavenumber 2μ. Finally, we numerically evaluate the integral quantities in (24) and obtain the complex amplitude of the streamfunction A_o from (23), where the detuning $\Delta\mu$ is defined as in (20) with $n_R = 3$.

The starred lines in Figs. 5a, b, c show the maximum value of the meridional profile of zonal wavenumbers 3 and 6 (defined, respectively, as $2|A_o|\max_\phi\{g(\phi)\}$ and $2|A_o|^2\max_\phi\{p(\phi)\}$) versus the strength of the zonal wind u for the three cases of Fig. 1. The numerical solutions obtained with NT = 6 and $J = 20$ are reported (thick solid lines) for a better comparison. Also reported (thin solid lines) are the predictions obtained from the linear resonance theory, which, of course, has zero amplitude in the zonal wavenumber 6. In general, the theory is able to qualitatively predict the folding of resonance; in the case of the climatological wind profile (Fig. 5c) the theoretical solution consistently bends to the left, owing to the positive value of I_δ. It must be noted that the prediction of the BMSS theory would fail in this case.

The quantitative agreement with the numerical solution is good as long as A_o is not too large. In fact, the

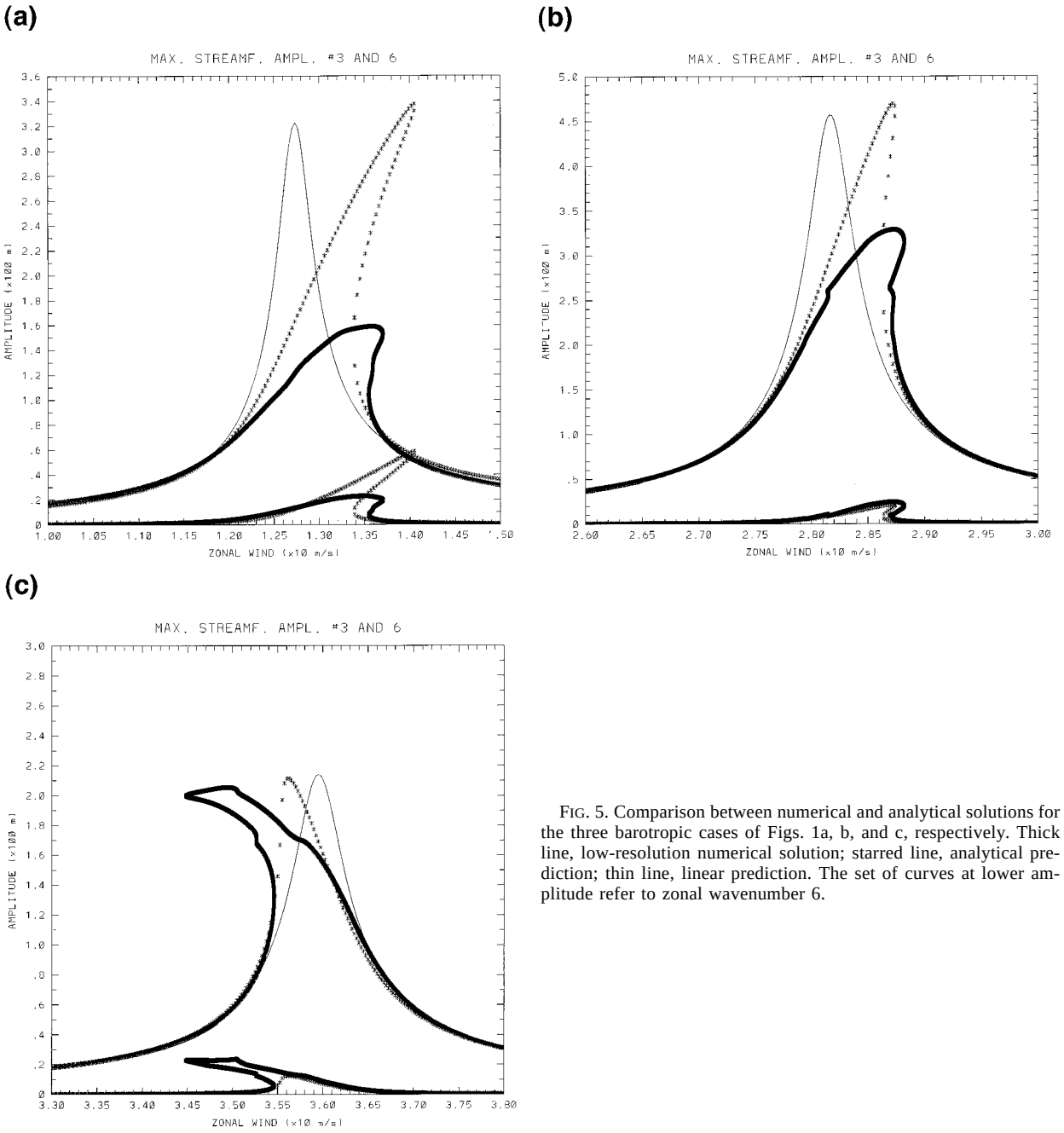

FIG. 5. Comparison between numerical and analytical solutions for the three barotropic cases of Figs. 1a, b, and c, respectively. Thick line, low-resolution numerical solution; starred line, analytical prediction; thin line, linear prediction. The set of curves at lower amplitude refer to zonal wavenumber 6.

weakly nonlinear theory breaks down when the streamfunction amplitude A_o is larger than order $h^{1/3}$, which is about 0.5 for the case of Fig. 5a. Significant discrepancies occur very close to resonance, especially in the case of Fig. 5a, where orographic forcing is probably too large to be considered really perturbative. This result is consistent with the sensitivity on resolution found, for this case, in section 2, which is an indication of the importance of nonlinearity in determining the maximum amplitude. Also notice that the bumps in Fig. 1a indicate the limit of validity of weakly nonlinear theory in a reasonable way.

Figure 6 reports the phase of zonal wavenumber 3 for the case of Fig. 5b, in which the theory performance is more satisfactory. As in the previous figure, the starred line denotes the prediction of the theory, the thick solid line represents the phase of (the wavenumber 3 component of) the numerical solution computed at the channel center, and the thin solid line is the linear theory prediction. The improvement introduced by the consid-

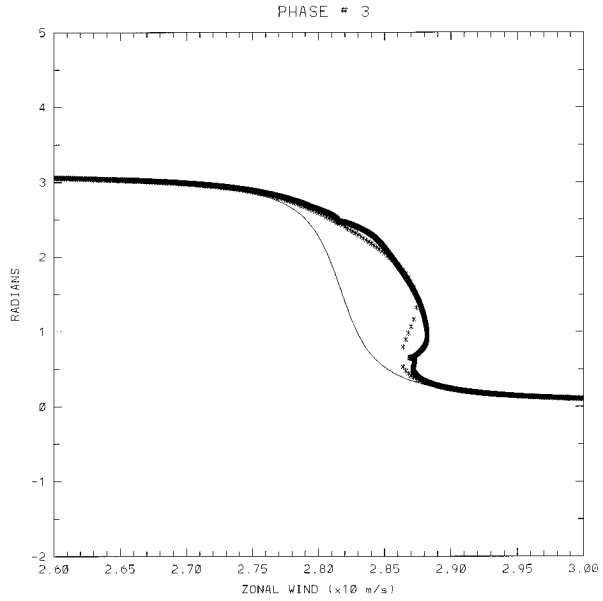

FIG. 6. Phase of zonal wavenumber 3 across resonance for the case of Fig. 5b.

eration of nonlinear effects in the linear resonance is evident. In this case, nonlinearity determines, at fixed u, a larger upstream displacement of the streamfunction highs with respect to orographic ridges. The opposite behavior is observed in the case of subresonant folding.

Finally, Figs. 7a,b show, respectively, the amplitude and phase of the zonal wavenumber 3 component of the upper-level streamfunction that corresponds to the two-level case studied at the end of section 3 (compare with Figs. 4a,b). The thick (thin) solid curve is relative to an orography of 50 (150) m of maximum height. The isolated branch of stationary solutions is predicted also by the weakly nonlinear theory for almost the correct value of the zonal wind but with a significantly larger amplitude. In the limit of zero orography, the isolated branch collapses to a point; in this case, the stationary Rossby wave is maintained against all forms of dissipations by baroclinic conversion of the available potential energy of the basic zonal wind. In fact, for this particular parameter setting, zonal wavenumber 3 is slightly unstable via ordinary baroclinic instability (not shown), with a phase speed that vanishes at a point very close to the value of u for which the stationary solution is found. As demonstrated by the linear approximation (dashed lines) in Fig. 7, nonlinearity plays a fundamental role in determining the existence of the large-amplitude solution.

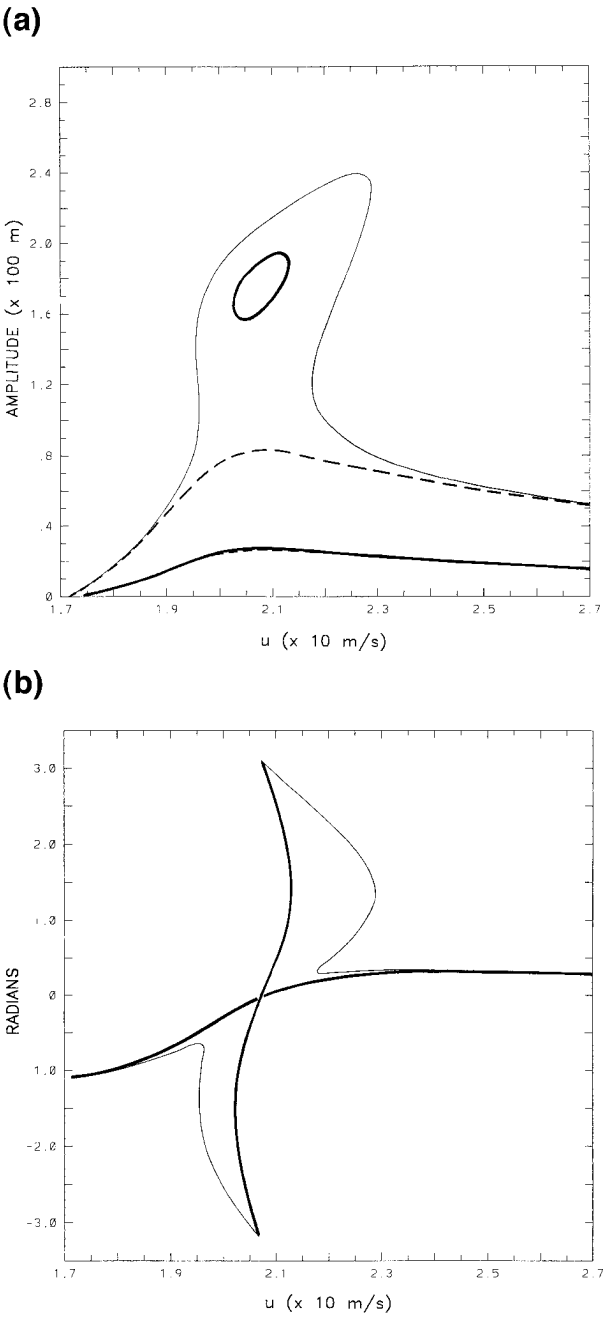

FIG. 7. Same as Fig. 4 but for the analytical solution. The dashed lines in (a) represent the linear approximation.

6. Discussion and conclusions

In this paper, we have checked the robustness of the mechanism of resonance folding, associated with nonlinear self-interaction of the wave field, by varying some geometrical and physical characteristics of the model presented in Part I. Our conclusion is that multiple, nonlinear equilibration of ultralong waves still stands out as a plausible dynamical ''skeleton'' able to explain one of the most relevant statistical properties of the low-frequency variability at midlatitudes, namely, that small variance of the zonal wind may correspond to large amplitude fluctuations of ultralong waves. We have also shown that the calculations presented in Part I are not sensitive to changes in horizontal resolution and phys-

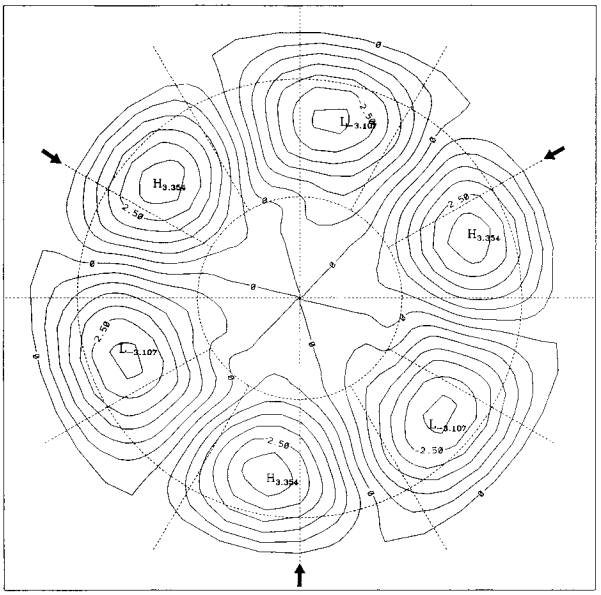

FIG. 8. Upper-level streamfunction (dimensionless) for the case of Fig. 3c with $u = 1.9$. The arrows indicate the position of orographic ridges. Contour interval is 0.5.

ical parameters. We have presented a revised theory for weakly nonlinear, orographically forced steady fields in the barotropic model. The qualitative agreement between weakly nonlinear and numerical solutions is satisfactory for all the cases investigated, provided the parameter values are consistent with the theory hypothesis.

One of the most unexpected results of the present work is the possibility of both super and subresonant foldings. This feature, also confirmed by the theoretical analysis of section 4, may open significant and interesting questions. From the physical point of view, there are differences between sub- and superresonant foldings that mainly concerns the phase of the stationary solutions. In the superresonant case (see Fig. 3b of Part I and the present Fig. 6), the large-amplitude equilibrium is almost out of phase with respect to topography, while the low-amplitude equilibrium is slightly ahead of it. The opposite situation is observed in the case of subresonant foldings, where large-amplitude solution anticyclones lie just ahead of orographic ridges. An example of a large-amplitude solution obtained in the subresonant folding case is depicted in Fig. 8, where the upper-level, eddy streamfunction pattern computed for $u = 1.9$ (high-resolution curve in Fig. 3c) is shown. As already pointed out in Part I, the presence of nonlinearity is also revealed by the steepening of the ridges and flattening of the troughs.

The change of folding type also implies changes in the stability properties of the stationary solutions. According to weakly nonlinear theory, a slow timescale instability must be expected in the large- and the small-amplitude solutions, while stability characterizes the intermediate one. All stationary solutions are anyway unstable in the present model, both via (modified) ordinary baroclinic instability and via barotropic instability of Rossby waves of the kind studied by Lorenz (1972), so that this weak, asymptotic instability is not likely to affect the dynamics around the equilibria.

Further investigation of stationary solutions, based on zonal wind profiles observed in different winter seasons, showed that both types of folding may occur in reality. If the structure of stationary states (and their stability) determines in some way the statistical properties of the system under examination (e.g., through clustering of the time-dependent solutions in the phase space regions nearby stationary solutions), then we should expect that the probability density function of the wave field be sensitive on the particular type of folding. This variability has already been noticed by Hansen and Sutera (1986) and by F. Molteni (1996, personal communication) in simple models. However, the connection between the two different foldings and the actual interannual variability of the probability density maxima remains, at this stage, highly speculative and must be supported by evidence both in time-dependent models of increasing complexity and in observations. In line of principle, the relation between the phase of quasi-stationary planetary waves and the type of resonance folding could be checked on atmospheric data, and work in this direction is presently in progress.

Acknowledgments. Support for this work was provided by the CEE Contract EV5V-CT93-0259.

REFERENCES

Benzi, R., P. Malguzzi, A. Speranza, and A. Sutera, 1986: The statistical properties of general atmospheric circulation: Observational evidence and a minimal theory of bimodality. *Quart. J. Roy. Meteor. Soc.,* **112,** 661–674.

Charney, J. G., and A. Eliassen, 1949: A numerical method for predicting the perturbation on the middle latitude westerlies. *Tellus,* **1,** 38–54.

——, and J. G. Devore, 1979: Multiple flow equilibria in the atmosphere and blocking. *J. Atmos. Sci.,* **36,** 1205–1216.

Hansen, A. R., and A. Sutera, 1986: On the probability density distribution of planetary-scale atmospheric wave amplitude. *J. Atmos. Sci.,* **43,** 3250–3265.

——, and ——, 1995: The role of topography in the low-frequency variability of the large-scale midlatitude circulation. *J. Atmos. Sci.,* **52,** 2497–2508.

Lorenz, E. N., 1972: Barotropic instability of Rossby wave motion. *J. Atmos. Sci.,* **29,** 258–264.

Malguzzi, P., A. Speranza, A. Sutera, and R. Caballero, 1996: Nonlinear amplification of stationary Rossby waves near resonance. Part I. *J. Atmos. Sci.,* **53,** 298–311.

Pedlosky, J., 1987: *Geophysical Fluid Dynamics.* Springer-Verlag, 710 pp.

Wiin-Nielsen, A., 1979: Steady states and stability properties of a low order, barotropic system with forcing and dissipation. *Tellus,* **31,** 375–386.